ELSEVIER

Earth and Planetary Science Letters 198 (2002) 211–224

EPSL

www.elsevier.com/locate/epsl

On the anatomy of mantle plumes: effect of the viscosity ratio on entrainment and stirring

Ichiro Kumagai *

Institute for Geothermal Sciences, Graduate School of Science, Kyoto University, Beppu 874-0903, Japan

Received 17 September 2001; received in revised form 28 January 2002; accepted 1 February 2002

Abstract

Laminar entrainment of starting plumes with compositional buoyancy has been explored in a series of laboratory experiments. Two types of starting plume have been identified within the range of viscosity ratio ε_{as} of 10.4–856 (defined as the ratio of the ambient to the buoyant fluid). The first type represents a vortex ring at small viscosity ratio ($\varepsilon_{as} < 11$) in which the plumes entrain the ambient fluids and form a rotating multi-layered structure within their heads. This is similar to the well-known structure observed in the thermal starting plumes of fluids having a strong temperature-dependent viscosity. In contrast, the second type of starting plume represents a more chaotic stirring regime at higher viscosity ratio ($104 < \varepsilon_{as} < 856$). Here, in the earlier stages, the plume head forms a double-layered structure by entrainment, with the buoyant fluid as the upper layer and the entrained fluid as the lower one. Thereafter, viscous coupling at the interface between the layers produces an intermediate stirring layer. This stirring layer grows with time with the end result that all fluids in the plume head mingle together. Using the fact that the resulting internal structure of the plume head depends on the viscosity ratio ε_{as} (a layered structure preserving the initial compositions vs. chaotic stirring tending towards homogeneity) a new viewpoint of mantle plume dynamics can be derived which is particularly useful in the interpretation of both spatial and temporal variations of geochemical data obtained from mantle plume products.

Keywords: mantle plumes; transport; mixing; laminar flow; laboratory studies

1. Introduction

Geological evidence such as topographic data and chronological studies of volcanic seamounts indicates a number of possible configurations for the external shapes of upwelling flows in the mantle (Fig. 1). For instance, the Deccan traps–Reunion hotspot [1] consists of the following sequence: a gigantic volcanic product of more than 10^6 km^3 generated in a geologically short span ($\sim$1 Ma) which was followed by a lower rate of production of magma (less than 1/10 of the initial rate) for tens of millions of years. This is thought to be the surface manifestation of a 'starting plume' (e.g. [1,2]) that consists of a large spherical head and a narrow conduit below (Fig. 1b). Recently, the technique of seismic

* Corresponding author. Present address: Department of Earth and Planetary Sciences, Tokyo Institute of Technology, Meguro, Tokyo 152-8551, Japan. Tel.: +81-3-5734-2336; Fax: +81-3-5734-3538.

E-mail address: kumagai@geo.titech.ac.jp (I. Kumagai).

0012-821X/02/$ – see front matter
PII: S0012-821X(02)00513-7

tomography has had great success in detecting such mantle plumes. For example, seismic images obtained from P- and S-waves under Iceland show a cylindrical region of low velocity [3], extending from the surface to the core–mantle boundary [4].

In the last two decades, the anatomy (internal structure) of mantle plumes has been the subject of research because geochemical studies of mantle plume products have revealed that they consist of more than two components from geochemically distinct sources (e.g. [5]). This multi-compositional structure is generally interpreted as indicating entrainment and mixing between plume sources and ambient mantle materials. However, the observational evidence, such as images derived from seismic tomography, is not able to reveal the small-scale structure and heterogeneity within a mantle plume. Furthermore, a seismic image represents only a snapshot of the present Earth's interior so that the formation process of such heterogeneity remains uncertain. Hence a fluid dynamical approach is useful for understanding the dynamical motion and precise structure of the plumes.

There are many fluid dynamical studies concerning the entrainment of a starting plume which results in structural evolution within the plume head (e.g. [6,7]). Apart from a few cases [8–10], however, these works discuss only the case of turbulent starting plumes (like jets and fountains) such as smoke from a volcanic vent. The systematic work of Griffiths, however, examined laminar entrainment (Reynolds number $Re \ll 1$) to simulate mantle diapirs and plumes [11–13]. He conducted a sequence of experiments on laminar vortex rings (spherical blobs, Fig. 1a) with fluids at a temperature-dependent viscosity controlled by varying the contribution to the buoyancy from thermal and compositional inputs [13]. In his experiments, all vortex rings with thermal buoyancy entrained the ambient fluid while no entrainment was observed when no thermal buoyancy was supplied. In the case of thermal vortex rings with fluids at a temperature-dependent viscosity [11,12], the surrounding fluid obtains buoyancy

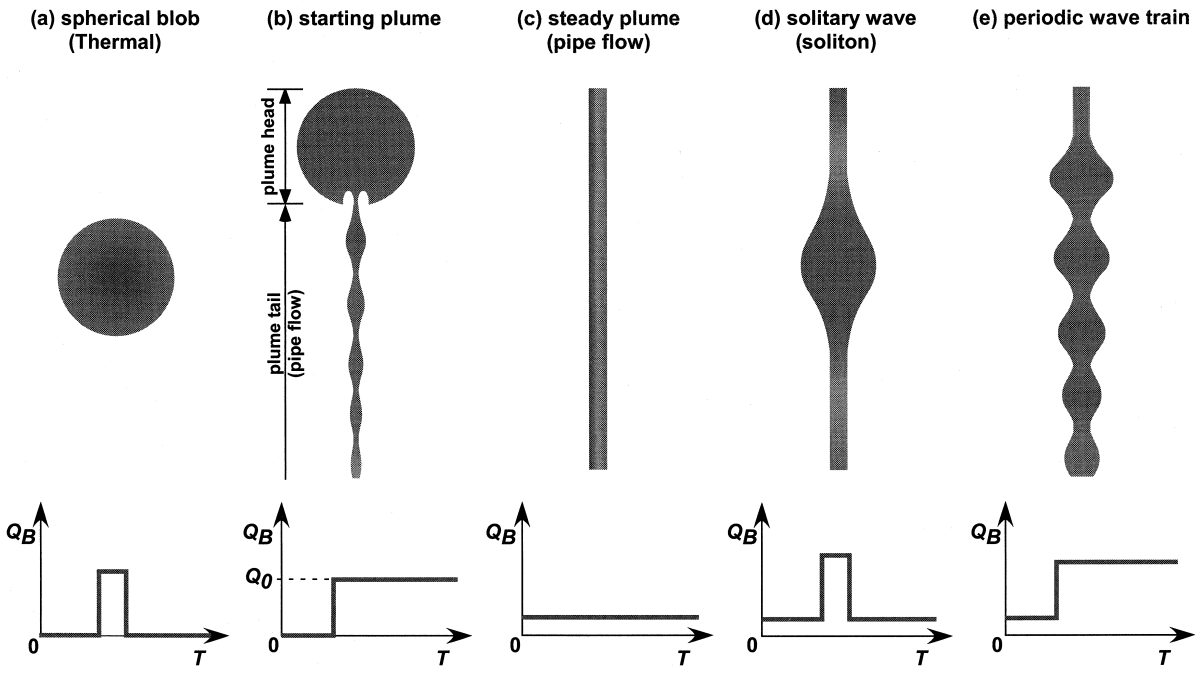

Fig. 1. Classification of the laminar upwelling flows for viscosity ratio $\varepsilon_{as} > 1$. Their morphology depends on the buoyancy flux Q_B as a function of time T. A starting plume (b) results from the initiation and then continued buoyancy injection (Q_0).

and decreases its viscosity by thermal diffusion. Therefore entrainment of the ambient fluid into the circulation flow within the thermal blob (vortex ring) takes place. Later, Griffiths and Campbell [8] expanded their study to starting plumes (Fig. 1b) with thermal buoyancy and experimentally demonstrated a large volume of entrainment. They also deduced that no obvious entrainment would occur in the case of a starting plume with compositional buoyancy [8] because of lack of thermal diffusion (or small molecular diffusion). (Note that Decoteau et al. demonstrated that a compositionally buoyant (CB) drop with large molecular diffusion entrained the ambient fluid at the bottom of the drop [14].) Recently, numerical experiments on thermally buoyant (TB) starting plumes with variable viscosity laws have been conducted (e.g. [15,16]) and these show that a large volume of the ambient fluid is entrained in the plume head when the fluid has a strongly temperature-dependent viscosity.

In contrast to TB starting plumes, CB starting plumes have little diffusion effect and so are hard to promote the entrainment phenomenon by the diffusive effects [11,12]. Nevertheless, entrainment phenomena with CB starting plumes have been observed in laboratory experiments. Before Griffiths' work, Whitehead and Luther [17] experimentally demonstrated entrainment within CB starting plumes, although Re was about 2 in their case. Within the creeping flow regime ($Re \ll 1$), small entrainment was observed in Olson and Singer's experiments on CB starting plumes [18] when the viscosity ratio ε_{as} of the ambient μ_a to the source μ_s fluids was approximately 1. Their starting plume (diapiric plume) exhibits a mushroom-like shape caused by the entrainment phenomenon but no spiral structure in the plume head. The entrainment phenomenon was also shown in the experiments of Loper and McCartney [19] and Loper et al. [20]. Their plumes entrained the ambient fluids at the bottom of the plume head. Neavel and Johnson [9] verified that large entrainment volumes can form with CB starting plumes when the viscosity ratio ε_{as} is between 0.7 and 6 by using both miscible and immiscible fluids. Their CB starting plume had a large spherical head with a vortex ring structure. In their experiments, no entrainment was observed when the viscosity ratio $\varepsilon_{as} > 18$. Recently, Kumagai and Kurita [21] have also found large volumes of entrainment for CB starting plumes at an ε_{as} value of 11 by supplying a small mass flux of the buoyant fluid at the source. These provide the motivation here to explore the mechanical entrainment (not the case of the diffusive entrainment) and the effect of high ε_{as} on the entrainment phenomenon of laminar starting plumes.

The laminar entrainment phenomenon involving starting plumes at high viscosity contrast is an important and attractive problem in the field of not only fluid dynamics but also mantle dynamics. A high viscosity contrast between the mantle plume and the ambient mantle is expected if the thermal diffusion is less effective than the advection of heat in the system (high Prandtl number Pr) because the sources of the mantle plumes will be at high temperature and the plume material will have a temperature-dependent viscosity. In this paper, I focus on the effect of viscosity contrast on the anatomy of the plumes and discuss the mechanical entrainment of the starting plumes. I then relate the anatomy of the mantle plumes to the temporal and spatial variations of geochemical and seismological heterogeneities in the mantle.

2. Laboratory experiments

2.1. Apparatus and method

The experiments were conducted in an acrylic tank (tank size is shown in Table 1) filled with a viscous fluid. The reservoir tank containing the buoyant fluid was connected to a nozzle located at the base of the acrylic tank. Both buoyant and ambient fluids used in the experiments were mixtures of syrup and water. Their fluid properties such as density and viscosity are given in Table 1. Before running each experiment, the ascent velocity of air bubbles was measured for calibration of the ambient fluid viscosity μ_a [22]. The buoyant fluids were colored by the addition of red dye for easy visualization.

An isothermal (compositional) starting plume

Table 1
Fluid properties of mixtures (syrup and water) in the present experiment

Expt. No.	ρ_a (kg/m^3)	ρ_s (kg/m^3)	μ_a (Pa s)	μ_s (Pa s)	ε_{as}	$2r_0$ (m)	u_0 (m/s)	Re_{plume}	Re_{pipe}
A-1	1385	1336	3.18	0.306	10.4	0.00302	0.000435	0.00367	0.00574
A-2	1385	1336	3.41	0.327	10.4	0.00358	0.000588	0.00585	0.00860
A-3	1385	1336	3.64	0.35	10.4	0.00232	0.000231	0.00149	0.00205
A-4	1385	1336	3.64	0.33	11.0	0.00202	0.000186	0.00122	0.00152
A-5	1385	1336	3.68	0.33	11.2	0.00336	0.000514	0.00422	0.00699
A-6	1385	1336	3.68	0.33	11.2	0.00288	0.000377	0.00216	0.00440
A-7	1385	1336	3.68	0.33	11.2	0.00260	0.000307	0.00152	0.00323
B-1	1442	1378	342	3.22	106	0.00667	0.000271	0.0000678	0.000774
B-2	1442	1378	326	3.13	104	0.00434	0.000118	0.0000186	0.000225
B-3	1442	1378	371	3.38	110	0.00335	0.0000649	0.00000996	0.0000886
C-1	1442	1335	436	0.649	672	0.00569	0.00169	0.000172	0.0198
C-2	1442	1335	497	0.654	760	0.00522	0.00143	0.000132	0.0152
C-3	1442	1335	655	0.764	857	0.00356	0.000543	0.0000297	0.00338
C-4	1442	1335	557	0.732	760	0.00268	0.000322	0.0000194	0.00157
C-5	1442	1335	326	0.555	587	0.00527	0.00164	0.000127	0.021

Re_{plume}: maximum Re for a plume head ($=\rho_a U_{max} D_{max}/\mu_a$); U_{max}: maximum ascent velocity of a plume head; D_{max}: maximum diameter of a plume head; Re_{pipe}: Re for a pipe flow ($=2\rho_s u_0 r_0/\mu_s$); u_0: average velocity of a pipe flow ($=Q_0/\pi r_0^2$); tank size: group A, $0.12\times0.15\times0.6$ m high; groups B and C, $0.15\times0.15\times0.8$ m high.

was produced by lifting up the reservoir tank, which in turn increased mass flux of the buoyant fluid Q_0. A sudden and then sustained buoyancy injection generated a leading blob (plume head) and a thin conduit (plume tail) connecting the blob with the source.

Experimental images were recorded by a three-channel CCD video camera and analyzed on a personal computer. Vertical length scales on the front and rear of the tank were provided in order to measure the plume height $H(t)$ and the horizontal diameter of the plume head $D_m(t)$. The plume velocity of ascent $U_P(t)$ was calculated from the $H(t)$ data and applied wall corrections [22]. The radius of the pipe flow r_0 was also measured to estimate the mass flux of the buoyant fluid Q_0. The errors of the r_0 depend on the resolution of the experimental images and are $\sim$0.12 mm. Here Poiseuille flow is assumed in the trailing conduit with radius r_0 [17] and the mass flux of the buoyant fluid Q_0 when $\mu_a \gg \mu_s$ is:

$$Q_0 = \frac{(\rho_a - \rho_s) g \pi r_0^4}{8\mu_s} \quad (1)$$

where ρ_a and ρ_s are the ambient and source fluid densities. In the present experiments the mass flux Q_0 was nearly constant because the pipe radius r_0 above the nozzle remained constant for all runs and the height level dropped by the buoyant fluid in the reservoir tank was small.

2.2. Experimental parameters

This work aims at understanding the influence of the viscosity ratio on the mechanical entrainment. Therefore experiments were conducted in three groups of viscosity ratio ε_{as} (group A: $\varepsilon_{as} \approx 10$, group B: $\varepsilon_{as} \approx 100$, group C: $\varepsilon_{as} \approx 700$) with different values of mass flux Q_0 (Table 1). However, for the study of the entrainment of the starting plumes, it is important to consider some additional parameters that will affect the entrainment phenomena and morphology of the starting plumes. Here we discuss the following parameters: (1) dimensionless density difference between the ambient and buoyant fluids ($\Delta\rho^* = (\rho_a - \rho_s)/\rho_a$), (2) the ratio of the diffusivities of momentum to composition (a compositional Pr or Schmidt number Sc), and (3) the Re of the starting plumes.

The $\Delta\rho^*$ have an important influence on the entrainment phenomenon. If $\Delta\rho^*$ is large, the viscous entrainment will be retarded by the buoy-

ancy force. In this experiments, $\Delta\rho^*$ of groups A, B and C were 0.035, 0.044, and 0.074, respectively. These are smaller than the value of Neavel and Johnson's experiment (0.37). This may potentially influence the entrainment problem and give rise to the difference between experimental results of this study and Neavel and Johnson [9].

The *Pr* number also affects the entrainment phenomenon and the structure of the plume head. Large diffusive effect (small *Pr*) produces a thick buoyant boundary layer around the plume head and it promotes the entrainment of the ambient fluids. In general, the *Pr* number based on the compositional (molecular) diffusivity, i.e. the *Sc* number, is very large in the case of compositional experiments. Therefore the compositional experiments have an advantage over the thermal experiments because the *Pr* number of the mantle is extremely high, $Pr \sim O(10^{24})$. In this study, the thickness of the buoyant boundary layer was very thin over the time scale of the experiment, and hence all entrainment in the present experiments is due to viscous drag only.

For both the plume head and the pipe flow, *Re* numbers measured and all experiments were conducted within the creeping flow regime ($Re \ll 1$, Table 1). In order to simulate the laminar plume motion expected in the Earth's mantle, highly viscous fluids and a low mass flux of the buoyant fluid Q_0 were applied to the present experiments.

3. Experimental results

3.1. Image analysis of CB starting plumes

All CB starting plumes entrained the ambient fluid within the range $10.4 < \varepsilon_{as} < 856.7$. Two types of plume structure were identified depending on the viscosity ratio ε_{as}, while the mass flux of the buoyant fluid Q_0 did not significantly affect the type of plume development.

3.1.1. Vortex ring type (group A: $\varepsilon_{as} \approx 10$)

Fig. 2 shows typical images of group A type of behavior. The heavier ambient fluid (transparent) was entrained from the bottom part of the plume head. The plume head expanded with time both through continuous supply from the source through the pipe flow and by entrainment of the ambient fluid. Both the buoyant (colored) and the entrained fluids (transparent) circulated within the plume head and developed a multi-layered and volute structure. This structure corresponds to the 'mushroom shape' type demonstrated by Neavel and Johnson [9] and is quite similar to the TB starting plumes which ascend through fluids with temperature-dependent viscosity [8].

3.1.2. Chaotic stirring types (group B: $\varepsilon_{as} \approx 100$, and group C: $\varepsilon_{as} \approx 700$)

Fig. 3a,b represent typical experimental images showing group B and group C types of behavior,

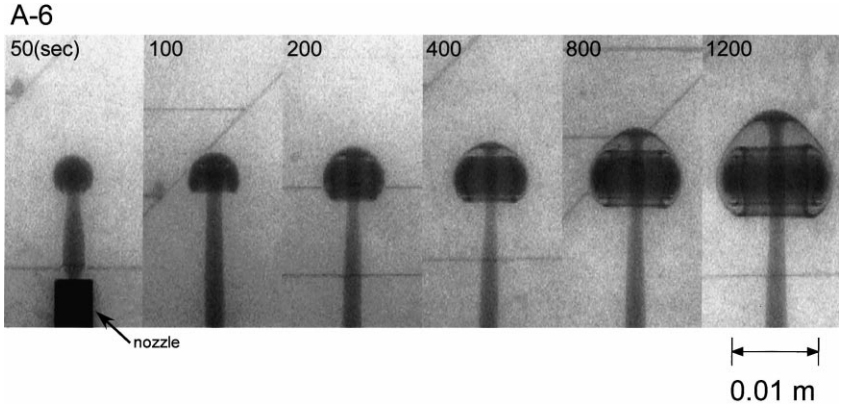

Fig. 2. Experimental images of a 'vortex ring' type plume (A-6 experiment). Viscosity contrast ε_{as} is 11. The ambient fluid (transparent) is entrained in the plume head and forms volute structure.

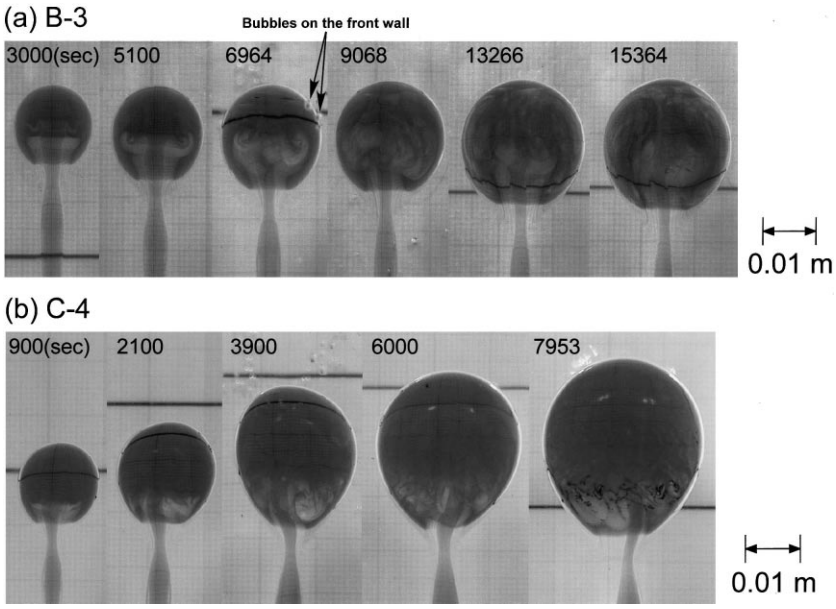

Fig. 3. Typical results from plumes in the 'chaotic stirring' type. (a) B-3 experiment ($\varepsilon_{as} = 110$). (b) C-4 experiment ($\varepsilon_{as} = 760$). Note that the grid lines on the rear side of the tank can be seen through the unmixed region of the plume head.

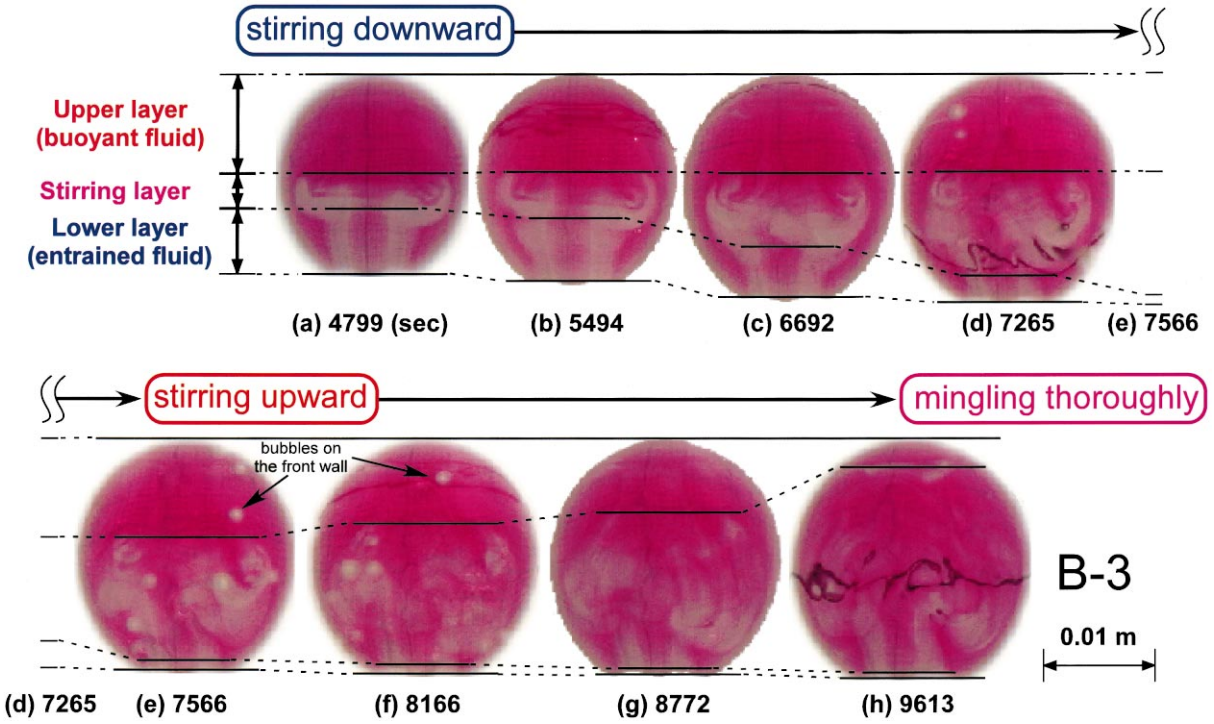

Fig. 4. Stirring process within a plume head of chaotic stirring type (B-3 experiment). The grid lines on the background wall are distorted by change of the refractive index due to the mingling process.

respectively. In the case of group B, the ambient fluid was also entrained from the bottom part of the plume head (as in group A), but this heavier material was unable to flow to the top of the plume head and remained stagnant in the lower regions. As a result, a double-layered structure was formed. However, this gravitational superposed structure was disturbed by viscous coupling between the upper and lower layers. As a new vortex emerged and grew at the interface a stirring region between the two layers started to develop. Fig. 4 shows this mingling process in a plume head and the evolution of these layers. At the earlier stage, the lower boundary of the stirring layer moved downward though the upper layer was almost stable (a–d). After the lower boundary of the stirring layer reached the bottom of the plume head (e), the upper boundary of the stirring layer migrated to the top of the plume head (e,f). Finally, the buoyant and entrained fluids mingled together and formed a chaotic structure within the plume head itself.

The starting plumes of group C also showed similar behavior to group B. However, the whole mingling was not observed in this case because the height of the tank was too short to observe the evolution of the plume in its entirety.

The mass flux Q_0 did not significantly affect the outline of this entrainment process; however, the quantitative values of the volume fraction of the ambient fluid in the plume head do depend on the value of Q_0 [23]. The whole mingling within the plume head was observed for the case of small Q_0 and long propagation distance.

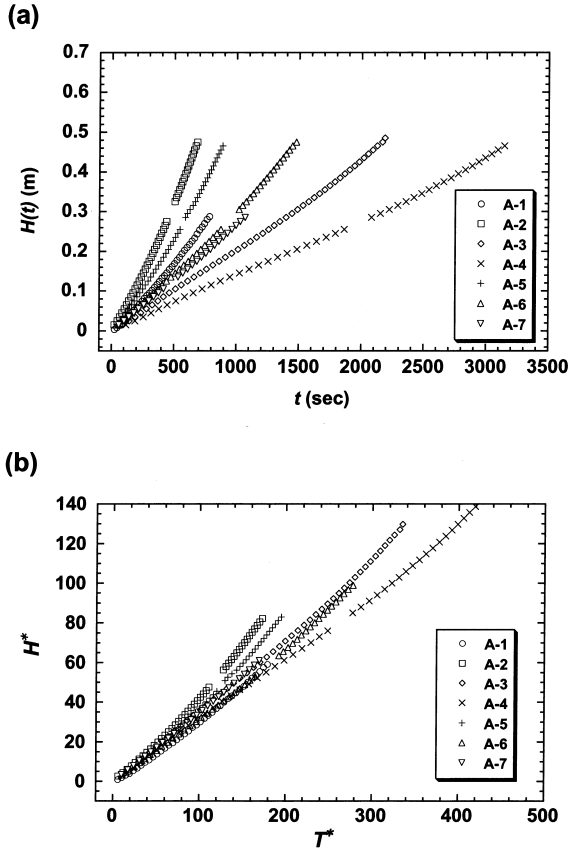

Fig. 5. (a) Height of the plume heads $H(t)$ for group A as a function of time t, and (b) normalized plots. $H^* = H(t)/R_0$ and $T^* = t/T_0$.

3.2. Height of the plume heads

The height reached by the plume heads $H(t)$ as a function of time t is shown in Fig. 5a for group A and in Fig. 6a for groups B and C. Larger values of the flux Q_0 cause higher velocities of ascent which result in shorter plume-head propagation times from the nozzle to the top of the experimental tank.

Figs. 5b and 6b show normalized height H^* as a function of normalized time T^*. The following time and length scales for normalization are used in these plots:

$$T_0 = \frac{\mu_a}{\Delta\rho_0 g r_0} \quad R_0 = r_0 \varepsilon_{as}^{\frac{1}{2}} \tag{2}$$

where $\Delta\rho_0 = \rho_a - \rho_s$. T_0 is the translation time for a Stokes' sphere of radius r_0 ascending through the layer of thickness r_0. The radius of a plume head is R_0, taken at the time when the ascent velocity of the plume head with no entrainment is equal to the average flow velocity of the buoyant fluid through the conduit $Q_0/\pi r_0^2$. All experimental results displayed a more or less linear behavior following this normalization, except for higher T^* and H^*. The discrepancy at this later stage (high T^* and high H^*) will originate from the large volume of entrainment which changes

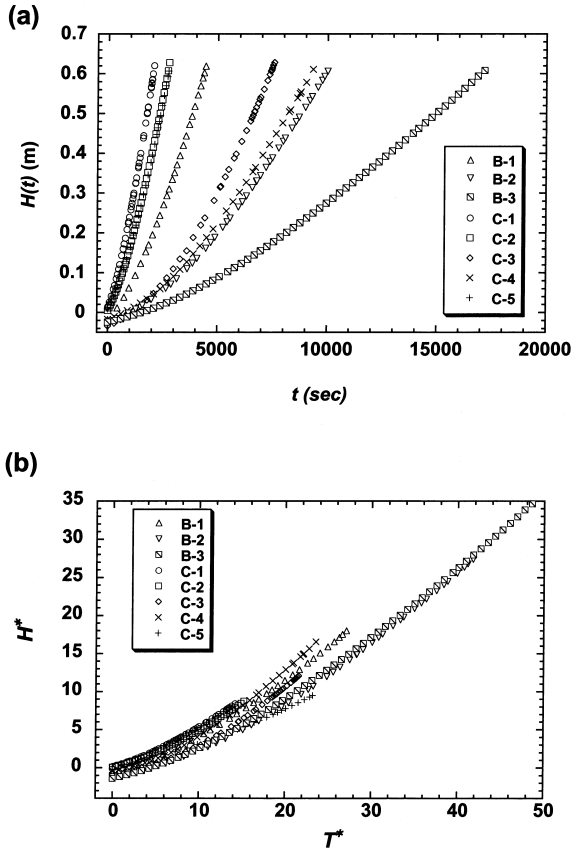

Fig. 6. (a) Height of the plume heads $H(t)$ for groups B and C as a function of time t, and (b) normalized plots. $H^* = H(t)/R_0$ and $T^* = t/T_0$.

the average viscosity of the plume head as well as the density.

3.3. Entrainment and mingling of the chaotic stirring type

The new type of the stirring observed here corresponds to a chaotic stirring process taking place at high viscosity ratio ε_{as}. The existence of a structural transformation from a *layered* regime to *stirring* regime is a notable feature of this new process (Fig. 3). Here, I discuss this transformation by introducing two parameters, *structural* volume fraction $\Phi_e(t)$ and *dynamic* volume fraction $\Phi_m(t)$, which are useful in representing the degree of entrainment and mingling, respectively.

The structural volume fraction $\Phi_e(t)$ is the net volume fraction of the entrained material $V_e(t)$ to the total volume of the plume head $V_{total}(t)$ (Fig. 7a). The $\Phi_e(t)$ is directly estimated from the experimental images by measuring the area ratio of the entrained material (light gray) to plume source (dark gray) in the plume head and also assuming an axisymmetric structure (Fig. 7a). Note that in

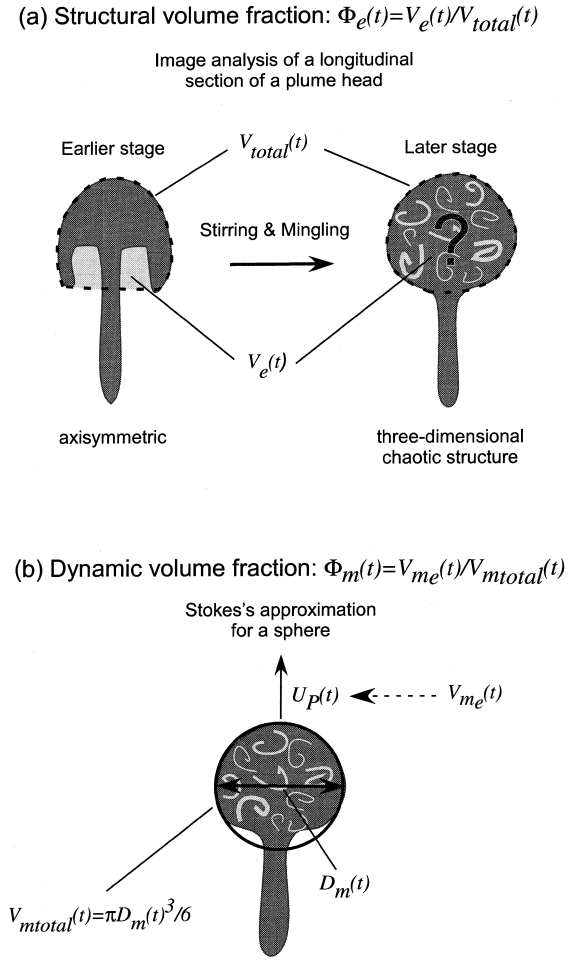

Fig. 7. The definitions and explanations of (a) structural volume fraction $\Phi_e(t)$ and (b) dynamic volume fraction $\Phi_m(t)$. The $\Phi_e(t)$ is the ratio of the volume of the entrainment within the plume head $V_e(t)$ (region in light gray) to the total volume of the plume head $V_{total}(t)$ (region within a dotted circle). It is difficult to estimate the entrained volume $V_e(t)$ of the later stage for the chaotic stirring type. The $\Phi_m(t)$ is determined by assuming the Stokes' approximation for the rate of ascent $U_P(t)$ of a sphere of diameter $D_m(t)$ (see Eq. 3 in the text).

the later stages of the plume development this assumption breaks down because the plume head entrains a large volume of the ambient fluid and shows a three-dimensional chaotic structure in the plume head.

The parameter $\Phi_m(t)$ is the dynamic volume fraction that is the ratio of the effective volume of entrainment $V_{me}(t)$ to the effective total volume of the plume head $V_{mtotal}(t) = \pi D_m(t)^3/6$ (Fig. 7b). In general, the ascent velocity of the plume head without entrainment is estimated from the Stokes' approximation for a sphere [17,24,25]. Neavel and Johnson assumed that this approximation is valid for the entrainment case and offset the velocity discrepancy between the entrainment and the no entrainment cases by introducing an effective (average) density for the plume head $\rho_m(t)$ [9]. Using this concept as a basis, Neavel and Johnson wrote the dynamic volume fraction of the entrained material in the plume head $\Phi_m(t)$ as:

$$\Phi_m(t) = \frac{V_{me}(t)}{V_{mtotal}(t)} = 1 - \frac{\Delta\rho_m(t)}{\Delta\rho_0} =$$

$$1 - \frac{12\mu_a U_P(t)}{(\rho_a - \rho_s) g D_m(t)^2} \quad \mu_a \gg \mu_s \qquad (3)$$

where $\Delta\rho_m(t) = \rho_a - \rho_m(t)$. The ascent velocity $U_P(t)$ and the horizontal diameter of the plume head $D_m(t)$ are obtained from the experimental data. This $\Phi_m(t)$ represents the effective volume fraction of the entrained material which influences the plume motion as a load.

We can now describe the structural evolution from layered to stirring stages observed in the experiments by using $\Phi_e(t)$ and $\Phi_m(t)$ values. Fig. 8 shows $\Phi_e(t)$ and $\Phi_m(t)$ for a typical B-3 experiment when the whole process of mingling in the plume head was observable. Firstly, at the layered stage (image of '3000 s' in Fig. 3a, $T^* \approx 8.5$), the value of $\Phi_m(t)$ is nearly equal to zero while $\Phi_e(t)$ continuously increases with time as shown in Fig. 8. This indicates that while entrainment phenomenon occurs in the plume head the entrained material does not affect the ascent velocity of the plume head. In other words, the plume head ascends through a viscous fluid without being influenced by the weight of the entrained material in the layered stage. Subsequently, in the stirring stage (> 3000 s in Fig. 3a), both $\Phi_e(t)$ and $\Phi_m(t)$ increase (Fig. 8) as stirring takes place at the interface between the two layers (Fig. 4). The value of $\Phi_m(t)$ approaches a constant value and finally all fluids in the plume head mingle thoroughly.

In short, the structural transformation within a plume head from layered stage to stirring stage observed in the chaotic stirring regime is best characterized by the dynamic volume fraction $\Phi_m(t)$ with $\Phi_m(t)$ ranging from zero to 0.15 (in case of B-3 experiment) for the progression from no stirring to the whole mingling. The onset time and the mechanism involved in this transformation may depend on the density difference $\Delta\rho^*$ and viscous drag force between the layers, but are still unclear.

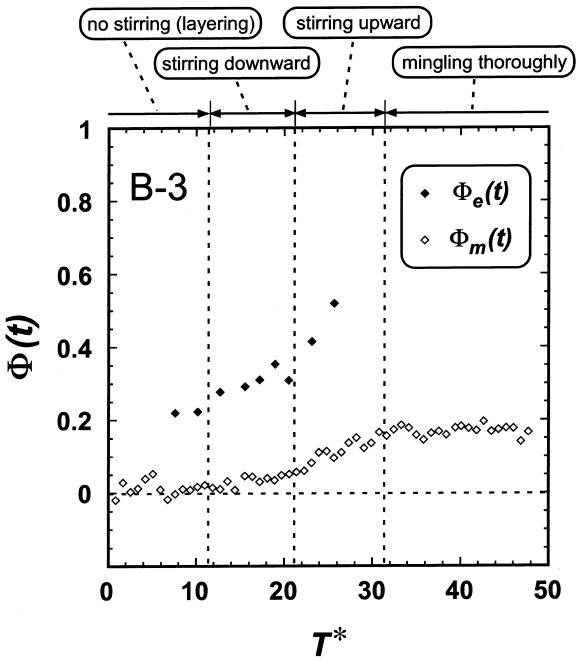

Fig. 8. Volume fraction of the entrained fluid in the plume head $\Phi(t)$ as a function of normalized time T^* (B-3 experiment). $\Phi_e(t)$ and $\Phi_m(t)$ were obtained from area measurements and Eq. 3, respectively. The $\Phi_m(t)$ is nearly zero at the layered stage ($T^* < 11.5$), but increases as stirring takes place and approaches a constant value.

4. Discussion and application to the Earth

4.1. 'Vortex rings' or 'chaotic stirring' in the mantle?

From a geophysical point of view, it is important to ask whether vortex rings or chaotic stirring should develop in the Earth's mantle. In the present experiments, the internal 'anatomy' of the plume head depends on the viscosity contrast of the ambient to the buoyant materials. Mantle materials have a temperature-dependent viscosity and plume source regions would be at a high temperature so that the plume material would be of lower viscosity. This causes a large viscosity contrast between mantle plumes and ambient mantle if the thermal diffusion effect is small (or large *Pr* number) and hence plumes of the chaotic stirring type could be expected in the mantle.

Alternatively, if the thermal diffusion effect is larger than that of heat advection (small *Pr* number), the viscosity contrast of the plumes becomes small and hence a vortex ring type would be expected (as with thermal starting plumes in fluids of a temperature-dependent viscosity as observed in the laboratory [8]). A fairly comprehensive work on entrainment by the diffusive effects has been done by Coulliette and Loper [10].

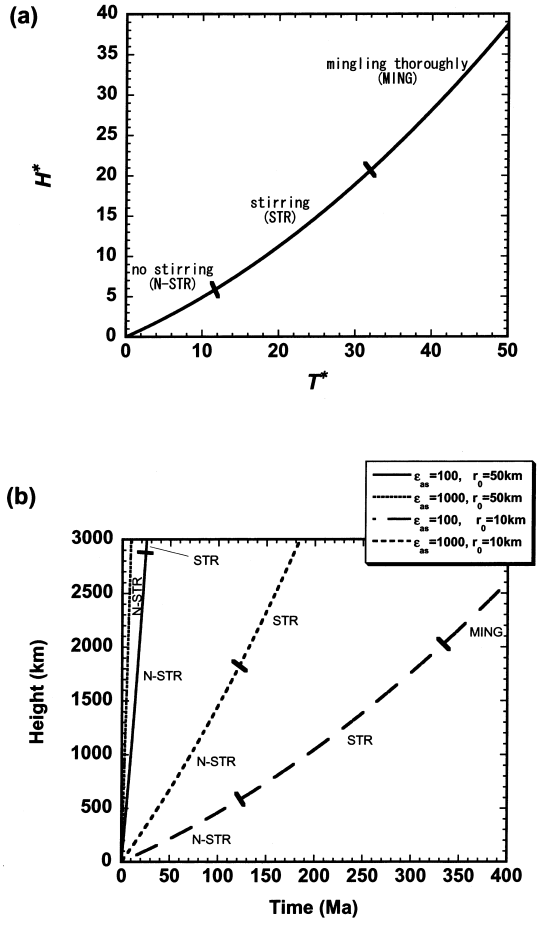

Fig. 9. (a) A non-dimensional curve of the plume ascent and the stirring behavior within the plume head for the chaotic stirring type. In the earlier stage, the plume head forms a double-layered structure (no stirring; N-STR). Thereafter, an intermediate stirring layer is produced by viscous coupling between the layers (STR) and finally all fluids in the plume head mingles thoroughly (MING). (b) The predicted heights of the starting plume heads for the chaotic stirring type under the mantle conditions; mantle viscosity $\mu_a = 10^{21}$ Pa s, density difference between the ambient and the buoyant materials $\Delta\rho_o = 30$ kg/m^3, and gravity acceleration $g = 10$ m/s^2. The predicted curves assume different viscosity ratios, ε_{as}, and the radii of the plume conduit r_0.

4.2. Starting plumes of chaotic stirring type under mantle conditions

The starting plumes of chaotic stirring type change their internal structure from no stirring to the whole mingling with their ascent (Fig. 9a. It is useful to consider what type of the internal structure of the plume head is expected under the mantle conditions and how the viscosity contrast ε_{as} affects the behavior of the mantle plumes. Here I attempt to make quantitative estimates for the behavior and internal structure of the mantle plumes of the chaotic stirring type. Fig. 9a shows a non-dimensional curve of the plume ascent for the chaotic mixing type and the stirring behavior within the plume head, which are experimentally determined. Fig. 9a and Eq. 2 can be used to extrapolate experimental results to mantle plumes, although values of the parameters in Eq. 2 have large uncertainties in the deep mantle.

For this simple estimation, I take $\mu_a = 10^{21}$ Pa s, $\Delta\rho_o = 30$ kg/m^3, and $g = 10$ m/s^2. Fig. 9b shows the height of rise of the mantle plume heads and the predicted structure within the plume heads. Four curves with different viscosity ratios ε_{as} and radii of the plume conduit r_0 are shown in

Fig. 9b. The style of the plume ascent and entrainment phenomenon vary strongly with both ε_{as} and r_0. The mantle starting plumes having large ε_{as} and r_0 (e.g. $\varepsilon_{as} = 1000$, $r_0 = 50$ km) ascend most rapidly and do not show the stirring phase through the whole mantle (~ 3000 km). This strong plume has a large mass flux ($Q_0 \approx 10$ km^3/yr) and maintains the stratified structure within the plume head. In contrast, in the case of small ε_{as} and r_0 (e.g. $\varepsilon_{as} = 100$, $r_0 = 10$ km), the structure within the mantle plume head evolves from no stirring to the whole mingling;

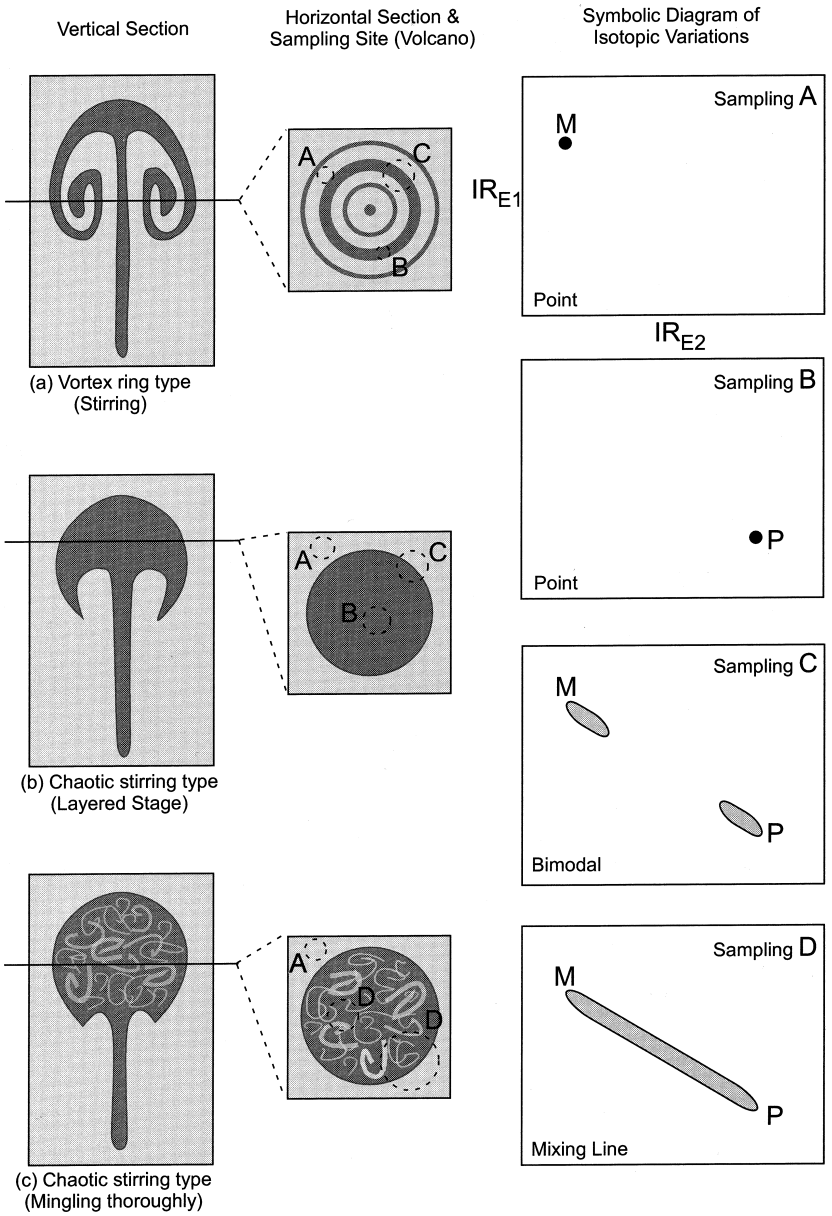

Fig. 10. Cartoons showing the morphology of starting plumes (left and middle columns) and spatial variations in plots of the isotopic ratios of IR_{E1} versus IR_{E2} (right column). M and P in the diagrams signify the end-members and the element concentration ratio E1/E2 is the same for both end-members.

however, the traveling time through the whole mantle is more than 400 Ma and the mass flux of the buoyant material is very small ($Q_0 \approx 10^{-3}$ km^3/yr), and hence this weak plume is unlikely to approach the Earth's surface.

4.3. Implications for plume anatomy and interpretation of geochemical data

Recent geochemical and seismological studies have dramatically improved our understanding of mantle plumes. The anatomy (internal structure) of starting plumes as it relates to the distribution of source material in the plume head is, however, a subject for future research. Here I attempt to deduce how the anatomy of the plumes observed in the present experiment might assist in the interpretation of geochemical observations and particularly in isotopic analysis of data showing temporal and spatial variations.

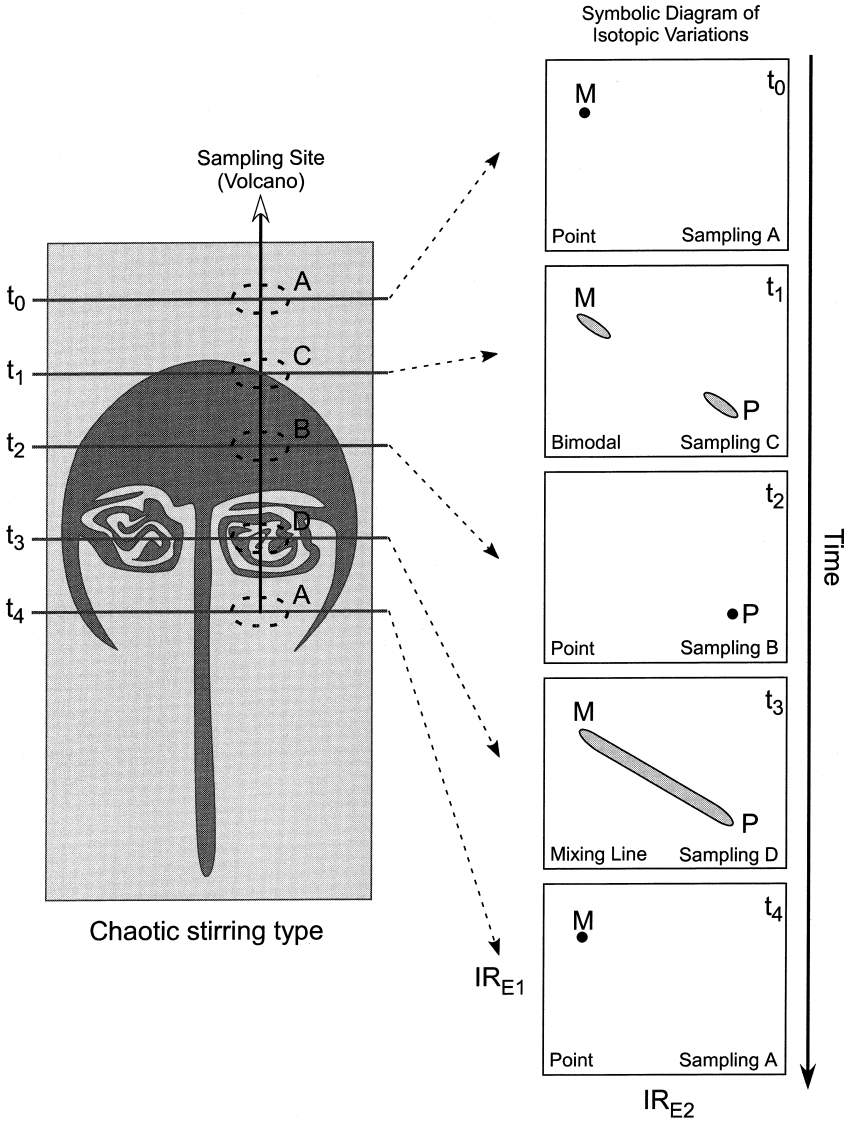

Fig. 11. Schematic illustration for anatomy of starting plumes (left) and temporal variation of isotopic diagrams from t_0 to t_4 (right). Other assumptions are the same as in Fig. 10.

Let us consider three types of starting plumes consisting of primitive plume sources (dark gray of Fig. 10) which are rising through the ambient mantle (light gray). In Fig. 10, the three scenarios are, respectively, (a) vortex ring type plume, which is observed when the viscosity ratio is low, (b) layered stage and (c) stirring stage for the chaotic stirring regime, which is observed when the viscosity ratio is high. Here, for simplicity, we assume that the resultant magma genesis occurs at around the middle level of the plume. The right column gives schematic illustrations of two-component mixing on a plot of the isotopic ratios RI_{E1} versus RI_{E2}. We also assume the special case that the relative element concentration ratio E1/E2 in the two end-members (ambient mantle M and plume source P) is the same, so that the mixing-line is straight. The dotted circles in the horizontal section (middle column) show the source regions for the volcano being sampled. No magma mixing is assumed during its ascent from the source to the surface.

The isotopic variation of the sampled magma (right column) depends on the extent of the magma source region, the size of the compositional band (middle column) and the degree of mixing. Samples from A and B are isotopically homogeneous because only one component is collected in the source region. Samples from C show a bimodal nature in the isotopic diagram since two components are collected. Sampling at D is the only case that shows a mixing-line with two end-members and derives from plume heads of the chaotic stirring type.

In addition to spatial variations, temporal variations can also be inferred from the isotopic diagrams. For instance, Fig. 11 shows the relation between a vertical section along a chaotic stirring type plume and temporal variation of the isotopic variation diagrams. Here we assume that magma is produced from the top (t_0) to the bottom (t_4) of the plume head as it is ascending. The related isotopic diagrams show a characteristic variation which reflects the anatomy of the plume head.

In order to provide an impetus for further work, I have attempted to connect the anatomy of the plume with isotopic signature, although many assumptions and considerable uncertainty are involved in this extrapolation. The above approach shows that the degree of mingling and the anatomy of the plume head are closely related to both temporal and spatial variations in isotopic signature. The topic of mantle plume anatomy is at the leading edge of geochemical and seismological research, and it is by understanding the relation between this anatomy and the available geological evidence that we will advance our understanding of mantle plume dynamics.

Acknowledgements

This paper has benefited from constructive comments of and discussions with K. Kurita, M. Jellinek and D.E. Loper. I.K. would like to acknowledge Y. Tatsumi, H. Yurimoto and S.D. King for their helpful support, and also J.P. Matthews for improving this manuscript. This research was financially supported by J.S.P.S. Research Fellowships. *[SK]*

References

[1] M.A. Richards, R.A. Duncan, V.E. Courtillot, Flood basalts and hot-spot tracks plume head and tails, Science 246 (1989) 103–107.
[2] W.J. Morgan, Convection plumes in the lower mantle, Nature 230 (1971) 42–43.
[3] C.J. Wolfe, I.T. Bjarnason, J.C. VanDecar, S.C. Solomon, Seismic structure of the Iceland mantle plume, Nature 385 (1997) 245–247.
[4] H. Bijwaard, W. Spakman, Tomographic evidence for a narrow whole mantle plume below Iceland, Earth Planet. Sci. Lett. 166 (1999) 121–126.
[5] S.R. Hart, E.H. Hauri, L.A. Oschmann, J.A. Whitehead, Mantle plumes and entrainment isotopic evidence, Science 256 (1992) 517–520.
[6] J.S. Turner, The 'starting plume' in neutral surroundings, J. Fluid Mech. 13 (1962) 356–368.
[7] J.S. Turner, Buoyant plumes and thermals, Annu. Rev. Fluid Mech. 1 (1969) 29–44.
[8] R.W. Griffiths, I.H. Campbell, Stirring and structure in mantle starting plumes, Earth Planet. Sci. Lett. 99 (1990) 66–78.
[9] K.E. Neavel, A.M. Johnson, Entrainment in compositionally buoyant plumes, Tectonophysics 200 (1991) 1–15.
[10] D.L. Coulliette, D.E. Loper, Experimental, numerical and analytical models of mantle starting plumes, Phys. Earth Planet. Inter. 92 (1995) 143–167.

[11] R.W. Griffiths, Thermals in extremely viscous fluids, including the effects of temperature-dependent viscosity, J. Fluid Mech. 166 (1986) 115–138.
[12] R.W. Griffiths, Particle motions induced by spherical convective elements in Stokes flow, J. Fluid Mech. 166 (1986) 139–159.
[13] R.W. Griffiths, The differing effects of compositional and thermal buoyancies on the evolution of mantle diapirs, Phys. Earth Planet. Inter. 43 (1986) 261–273.
[14] K.L. Decoteau, G. Achenbach, D. Loper, P. Arce, A preliminary characterization of puddle formation flows with experimental visualization, Proceedings of the Vth Latin American and Caribbean Congress on Fluid Mechanics, May 14–17, 2001, Universidad Simon Bolivar, Caracas, Venezuela, Paper # MPF-1.
[15] P. vanKeken, Evolution of starting plumes: a comparison between numerical and laboratory models, Earth Planet. Sci. Lett. 148 (1997) 1–11.
[16] L.H. Kellogg, S.D. King, The effect of temperature dependent viscosity on the structure of new plumes in the mantle: Results of a finite element model in a spherical, axisymmetric shell, Earth Planet. Sci. Lett. 148 (1997) 13–26.
[17] J.A. Whitehead, D.S. Luther, Dynamics of laboratory diapir and plume models, J. Geophys. Res. 80 (1975) 705–717.
[18] P. Olson, H. Singer, Creeping plumes, J. Fluid Mech. 158 (1985) 511–531.
[19] D.E. Loper, K. McCartney, Mantle plumes and the periodicity of magnetic field reversals, Geophys. Res. Lett. 13 (1986) 1525–1528.
[20] D.E. Loper, K. McCartney, G. Buzyna, A model of correlated epsodicity in magnetic-field reversals, climate, and mass extinctions, J. Geol. 96 (1988) 1–15.
[21] I. Kumagai, K. Kurita, Laboratory experiment on entrainment and lifecycle of the starting plume, Abstract of the 6th SEDI Symposium, Tours, France, 1998, p. 183.
[22] J. Happel, H. Brenner, Low Reynolds Number Hydrodynamics, 2nd edn., Noordhoff, Leiden, 1973.
[23] I. Kumagai, K. Kurita, On the fate of mantle plumes at density interfaces, Earth Planet. Sci. Lett. 179 (2000) 63–71.
[24] G.K. Batchelor, An Introduction to Fluid Dynamics, Cambridge University Press, Cambridge, 1967.
[25] B.D. Marsh, Island arc development: some observations, experiments and speculations, J. Geol. 87 (1979) 687–713.